Received: 5 September 2016 | Revised: 17 October 2016 | Accepted: 20 October 2016

DOI: 10.1002/bio.3256

WILEY LUMINESCENCE
The Journal of Biological and Chemical Luminescence

RESEARCH ARTICLE

Crystal structure and luminescence properties of the blue-green-emitting $Ba_9(Lu, Y)_2Si_6O_{24}:Ce^{3+}$ phosphor

Huawei Xu[1] | Zhi Zhou[2] | Yongfu Liu[3] | Qunxing Liu[1] | Zhiyuan He[1] | Shen Wang[1] | Linyi Huang[1] | Hongbo Zhu[4]

[1] The Fifth Research Institute of MIIT, Quality Inspection and Testing Center, No. 110 Dongguan Zhuang Road, Guangzhou, China

[2] College of Science, Hunan Agricultural University, No. 1 Nongda Road, Changsha, China

[3] Ningbo Institute of Materials Technology and Engineering (NIMTE), Chinese Academy of Sciences (CAS), No. 1219 Western Zhongguan Road, Ningbo, China

[4] Changchun Institute of Optics, Fine Mechanics and Physics, Chinese Academy of Sciences, No. 3888, Nanhu Road, Changchun 130033, China

Correspondence
Huawei Xu, The Fifth Research Institute of MIIT, Quality Inspection and Testing Center, No. 110 Dongguan Zhuang Road, Guangzhou 510610, China.
Email: xhw@ceprei.biz

Zhi Zhou, College of Science, Hunan Agricultural University, No. 1 Nongda Road, Changsha 410128, China.
Email: zhouzhi@hunan.edu.cn

Yongfu Liu, Ningbo Institute of Materials Technology and Engineering (NIMTE), Chinese Academy of Sciences (CAS), No. 1219 Western Zhongguan Road, Ningbo 315201, China.
Email: liuyongfu@nimte.ac.cn

Funding information
National Natural Science Foundation of China, Grant/Award Number: 11404351, U1201254 and 61306059. National High Technology Research and Development Program of China (863 Program), Grant/Award Number: 2015AA03A101. Science and Technology Planning Project of Guangdong Province, Grant/Award Number: 2014B010122005, 2014B010122001, 2015B010114002 and 2015B010133001

Abstract

Samples of the $Ba_9(Lu_{2-x}Y_x)Si_6O_{24}:Ce^{3+}$ (x = 0–2) blue-green phosphors were synthesized by solid-state reactions. All the samples exhibited a rhombohedral crystal structure. As the Y^{3+} concentration increased, the diffraction peaks shifted to the small angle region and the lattice parameters increased due to the larger ionic radius of Y^{3+} (r = 0.900 Å) compared with that of Lu^{3+} (r = 0.861 Å). Under 400 nm excitation, samples exhibited strong blue-green emissions around 490 nm. The emission bands had a slight blue shift that resulted from weak crystal-field splitting with increasing Y^{3+} concentration. Luminescence intensity and quantum efficiency (QE) decreased with increasing Y^{3+} concentration. The internal QE decreased from 74 to 50% and the external QE decreased from 50 to 34% as x increased from 0 to 2. The thermal stability of the Lu series was better than that of the Y-series. The excitation band peak around 400 nm matched well with the emission light from the efficient near-ultraviolet (NUV) chip. These results indicate promising applications for these NUV-based white light-emitting diodes.

KEYWORDS

blue-green phosphor, Ce^{3+} luminescence, near ultraviolet, silicate, white LEDs

1 | INTRODUCTION

White light-emitting diodes (WLEDs) have drawn much attention in the field of general illumination due to their advantages of high efficiency, energy savings, environmental friendliness, and long service lifetime, etc.[1–7] The commercial WLED commonly consists of a yellow-emitting phosphor $Y_3Al_5O_{12}:Ce^{3+}$ (YAG:Ce^{3+}) and a blue-emitting LED chip. However, YAG:Ce^{3+} lacks red spectral components, thus resulting in a low color rending index (CRI < 70) and a high correlated color temperature (CCT > 6500 K).[8–10] Moreover, the blue light provided by LED chips is closely related to the working current leading

Abbreviations: CAS, Chinese Academy of Sciences; CRI, color rending index; NIMTE, Ningbo Institute of Materials Technology and Engineering; NUV, near ultraviolet; QE, quantum efficiency; XRD, X-ray powder diffraction.

to an unstable color hue. These drawbacks meant that YAG:Ce^{3+} failed to meet indoor lighting requirements that prefer a warm white light with a low CCT (<4000 K) and a high CRI (>80). As an alternative scheme, the combination of a near-ultraviolet (NUV) LED chip and three-primary color (red, green, and blue) phosphors can generate an ideal white light with a high CRI and a tunable CCT.[11–18] In addition, the color of NUV-based WLEDs is only decided by phosphors, which circumvent the color drift under a fluctuation of working current. Thus, researchers have recently focused on novel NUV excited phosphors with excellent luminescence properties and the solid-state solution is an effective method to achieve novel phosphors.[19,20]

Rare-earth doped orthosilicate phosphors have attracted much attention due to their excellent luminescence for the NUV-based WLEDs.[21–32] For instance, the novel blue-green phosphor $Ba_9Lu_2Si_6O_{24}:Ce^{3+}$ (BLS:Ce^{3+}) even has a high efficiency as nitride phosphors.[28] However, BLS:Ce^{3+} is more easily synthesized than nitride phosphors. As known, $Ba_9Y_2Si_6O_{24}:Ce^{3+}$ (BYS:Ce^{3+}) is also an efficient blue-green phosphor that has the same crystal structure with $Ba_9Lu_2Si_6O_{24}:Ce^{3+}$.[25] In this study, we synthesized a series of the $Ba_9(Lu_{2-x}Y_x)Si_6O_{24}:Ce^{3+}$ phosphors. Based on the X-ray powder diffraction (XRD), changes in crystal structure were studied. The photoluminescence (PL), photoluminescence excitation (PLE), internal and external QE, absorbance, and thermal stability of all the samples are discussed.

2 | EXPERIMENTAL

Samples of $Ba_9(Lu_{2-x}Y_x)Si_6O_{24}$:5%$Ce^{3+}$ (x = 0–2) were prepared by the conventional high temperature solid-state reaction. The starting materials ($BaCO_3$, 99.8%; Lu_2O_3, 99.99%; Y_2O_3, 99.99%; SiO_2, 99.9%; CeO_2, 99.99%) were all weighted out in the desired stoichiometry and thoroughly mixed using an agate mortar and pestle for 40 min. The mixed powders were placed in an alumina crucible and sintered in a tube furnace under reducing atmosphere (95%N_2 + 5%H_2) at 1500°C for 5 h. After cooling to room temperature, the products were subsequently ground to a fine powder with an agate mortar and pestle for further analysis.

XRD data were collected for all samples on a Bruker D8 Advance diffractometer with Cu Kα radiation (λ = 1.54056 Å) at 40 kV and 40 mA. PL and PLE spectra were obtained on a Hitachi F-4600 spectrometer equipped with a 150 W Xenon lamp under a working voltage of 400 V. The internal and external QEs and the dependence of QEs on temperature were measured using a QE-2100 spectrophotometer from Otsuka Photal Electronics. Photographs of the samples under sunlight or a 365 nm ultraviolet (UV) lamp were taken using a Nikon D90 camera.

3 | RESULTS AND DISCUSSION

Figure 1 shows the XRD patterns in the range 10–80° for the samples of $Ba_9(Lu_{2-x}Y_x)Si_6O_{24}$:5%$Ce^{3+}$ (x = 0–2). It can be seen that all of these exhibited the same single crystal phase with the profile of $Ba_9Sc_2Si_6O_{24}$ (PDF No. 82–1119) and no impurity phase was observed. Previously, we have demonstrated that BLS and BYS have the same rhombohedral structure.[25,28] Figure 1 indicates that the crystal phase does not change when Lu and Y coexist in the same host. This rhombohedral structure, shows an $R\bar{3}$ symmetry. There are three

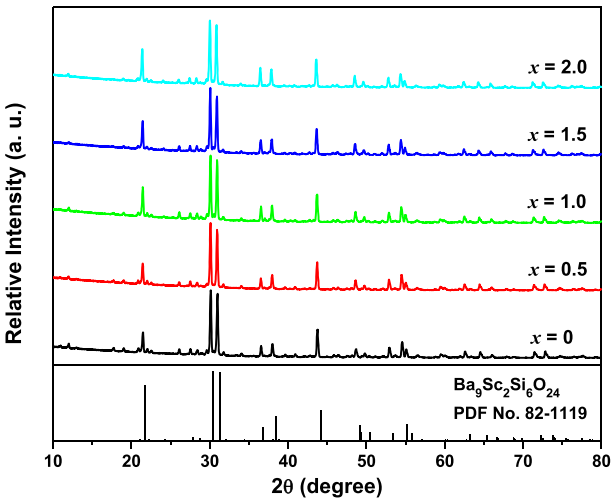

FIGURE 1 XRD patterns (2θ = 10–80°) for $Ba_9(Lu_{2-x}Y_x)Si_6O_{24}$:5%$Ce^{3+}$ with x = 0–2

independent barium sites in this structure, which are Ba(1), Ba(2), and Ba(3) coordinated with 12, 9, and 10 oxygen atoms, respectively. There is only one site for Lu/Y and Si coordinated with 6 and 4 oxygen atoms, respectively. Both the Ba and Lu/Y sites can be occupied when Ce is incorporated into this structure.[25,28]

Figure 2 shows the XRD patterns in the range of 29–32° for the samples of $Ba_9(Lu_{2-x}Y_x)Si_6O_{24}$:5%$Ce^{3+}$ (x = 0–2). It is noted that the diffraction peak shifts to small angle region with x increasing. This should be ascribed to the larger ionic radius of Y^{3+} (r = 0.90 Å, six-coordinated) rather than that of Lu^{3+} (r = 0.861 Å, six-coordinated). With increase in Y^{3+} content, the crystal volume enlarges gradually, thus the diffraction peak shifts to the small angle region. The lattice parameters of a, c, and V were calculated based on the XRD data, as shown in Figure 3. It can be seen that the shift of the diffraction peaks and the lattice parameters are almost linearly dependent on the x value. According to Vegard's law, therefore, we believe that Lu and Y form a solid solution when they coexist in the titled matrix.

Figure 4 displays the PL (λ_{ex} = 400 nm) and PLE (λ_{em} = 490 nm) spectra for $Ba_9(Lu_{2-x}Y_x)Si_6O_{24}$:5%$Ce^{3+}$ with x = 0–2. For the PLE spectra, the excitation band from 200 to 370 nm is from the Ce^{3+} at the Ba^{2+}

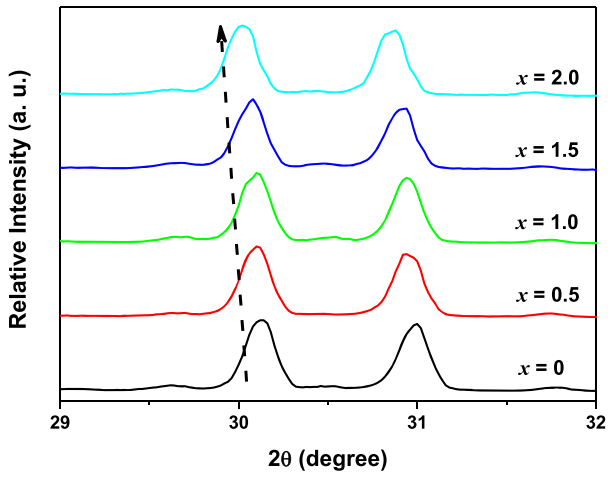

FIGURE 2 XRD patterns (2θ = 29–32°) for $Ba_9(Lu_{2-x}Y_x)Si_6O_{24}$:5%$Ce^{3+}$ with x = 0–2

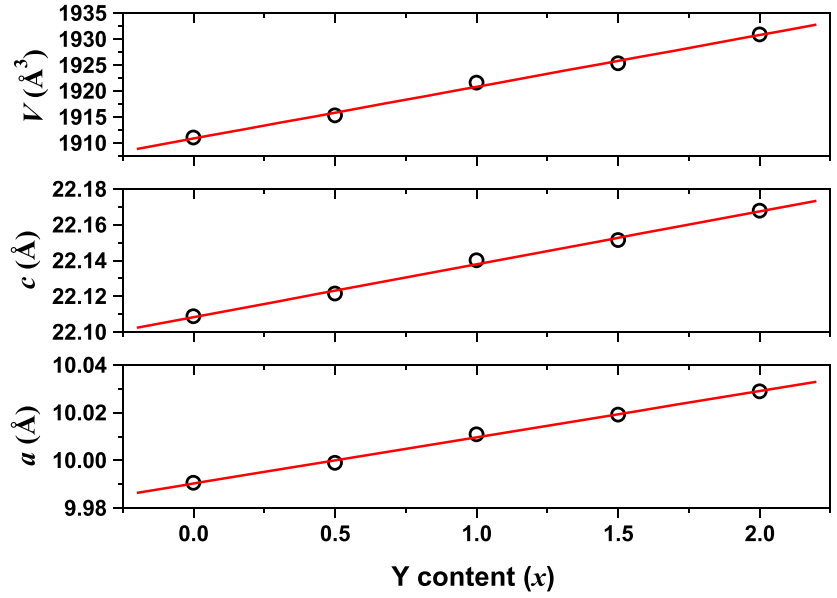

FIGURE 3 Calculated lattice parameters of *a*, *c*, and *V* for $Ba_9(Lu_{2-x}Y_x)Si_6O_{24}$:5%$Ce^{3+}$ with x = 0–2

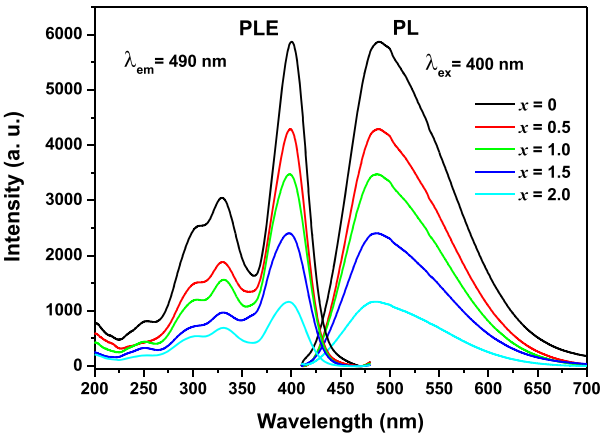

FIGURE 4 PL (λ_{ex} = 400 nm) and PLE (λ_{em} = 490 nm) spectra for $Ba_9(Lu_{2-x}Y_x)Si_6O_{24}$:5%$Ce^{3+}$ with x = 0–2

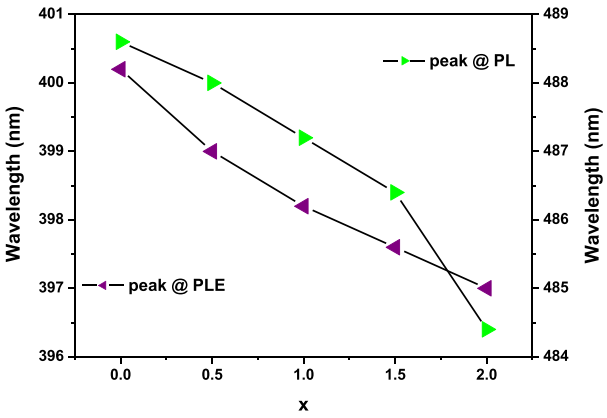

FIGURE 5 Peak wavelengths of PL and PLE spectra for $Ba_9(Lu_{2-x}Y_x)Si_6O_{24}$:5%$Ce^{3+}$ with x = 0–2

site, while the strong band peaking around 400 nm is from the Ce^{3+} at the Lu/Y site.[25,28] The 400 nm excitation band matches well with the emission light (390–410 nm) of the efficient NUV chips. Thus, this kind of phosphor exhibits potential application for NUV-based white LEDs. Under 400 nm excitation, the samples show blue-green emissions peaking around 490 nm with a band width of about 116 nm. The emission arises from the transition of the lowest 5d state to the $^2F_{7/2}$ and $^2F_{5/2}$ ground states. Thus, the emission is composed of two Gaussian bands peaking at 482 nm (20 750 cm^{-1}) and 536 (18 650 cm^{-1}) nm with an energy difference of about 2100 cm^{-1}, consistent with the energy difference between the $^2F_{7/2}$ and $^2F_{5/2}$ ground states (~2200 cm^{-1}). However, the emission intensity decreases gradually with increasing Y^{3+} contents.

Figure 5 depicts the peak wavelengths of the PL and PLE spectra for $Ba_9(Lu_{2-x}Y_x)Si_6O_{24}$:5%$Ce^{3+}$ with x = 0–2. The emission peak shifts from 488.6 to 484.4 nm when x increases from 0 to 2. The excitation peak shifts from 400.2 to 397 nm when x increases from 0 to 2. Clearly, both of these shift to a small wavelength with increasing Y^{3+} content. The CIE color coordinates based on the PL spectra in

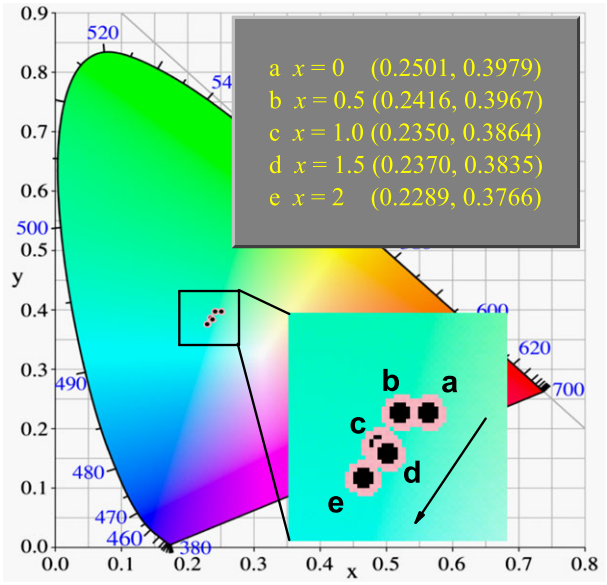

FIGURE 6 CIE color coordinates for $Ba_9(Lu_{2-x}Y_x)Si_6O_{24}$:5%$Ce^{3+}$ with x = 0–2

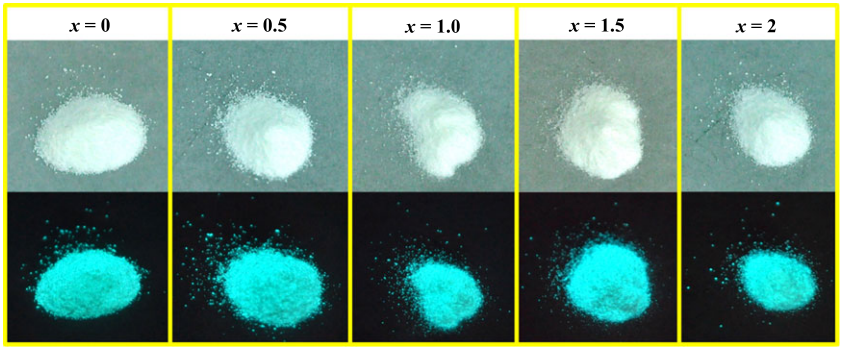

FIGURE 7 Photographs of the $Ba_9(Lu_{2-x}Y_x)Si_6O_{24}$:5%$Ce^{3+}$ (x = 0–2) samples under sunlight (up) or 365 nm UV lamp (down)

Figure 4 are also depicted in Figure 6. Images of all the samples under sunlight or 365 nm UV light are given in Figure 7.

All the samples show a while color under sunlight and a blue-green color under 365 nm UV light. The color differences are not apparent. However, the color coordinates shift from (0.2501, 0.3979) for x = 0 to (0.2289, 0.3766) for x = 2.0, as depicted in Figure 7. This blue shift should be attributed to the smaller Y^{3+} ions. As known, blue-green emission is from the 5d → 4f transition of Ce^{3+}, and the position of the lowest 5d energy level is strongly dependent on the crystal-field strength. Furthermore, crystal-field splitting, Dq, has an inverse relationship with the bond length, R, in the unit cell, and can be expressed by equation 1:

$$Dq = \frac{Ze^2r^4}{6R^5} \quad (1)$$

where Z is the anionic charge, e is the charge of the electron, and r is the radius of the 5d–wave function.[33] The unit cell increases gradually with the increasing substitution of Y^{3+} for Lu^{3+}, as demonstrated in Figure 3, due to the larger Y^{3+} than Lu^{3+}, which leads to the longer bond length and the larger R value. Thus the crystal-filed strength becomes weaker and then the crystal-field splitting becomes smaller. In this condition, the lowest 5d energy level is promoted, therefore, the luminescence of Ce^{3+} shows a blue-shift behavior when the sample changes from the Lu series to the Y-series.

The internal QE (η_{int}) is also called the fluorescence quantum yield (Φ_F), which is the ratio of emitted photons and the number of only absorbed photons.[34] The external QE (η_{ext}) is the ratio of emitted photons to the number of incident photons, called absolute quantum yield.[30,35–38] Their relationship can be described as the following:

$$\eta_{ext} = \frac{N_{em}}{N_{inc}}\,\eta_{int} = \frac{N_{em}}{N_{abs}}\,\eta_{ext} = A\eta_{int} \quad (2)$$

where N_{inc}, N_{abs} and N_{em} are the number of incident, absorbed and emitted photons, respectively. A is the absorbance. Equation 2 is a direct method to evaluate the practical QE, which can be obtained by the QE-2100 quantum efficiency measurement system mentioned in the Experimental section. Figure 8 shows the internal and external QEs for $Ba_9(Lu_{2-x}Y_x)Si_6O_{24}$:5%$Ce^{3+}$ (x = 0–2) under 400 nm excitation. With increasing Y^{3+} content, the internal QE decreased from 74 to 50%, and the external QE decreased from 50 to 34%. These phenomena are similar to the changes in luminescence intensities shown in Figure 4. Based on the relationship between external and internal QEs, the absorbance (A) of samples can be expressed as A = external

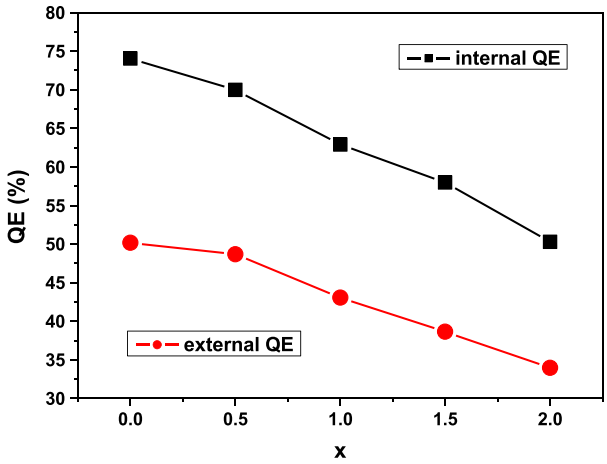

FIGURE 8 Internal and external QEs for $Ba_9(Lu_{2-x}Y_x)Si_6O_{24}$:5%$Ce^{3+}$ (x = 0–2) under 400 nm excitation

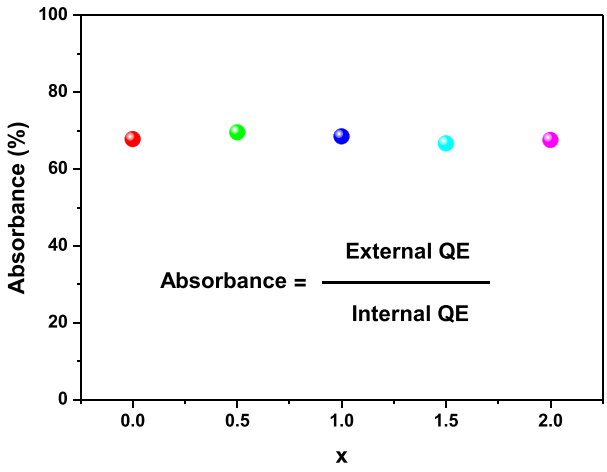

FIGURE 9 Dependence of absorbance on Y^{3+} content in $Ba_9(Lu_{2-x}Y_x)Si_6O_{24}$:5%$Ce^{3+}$ (x = 0–2)

QE/internal QE.[30] The dependence of A on Y^{3+} content x is depicted in Figure 9. It can be seen that the absorbance is around 68% and almost does not change with Y^{3+} content. For thermal stability at 150°C, nearly 88% of the internal QE at room temperature can be maintained for BYS:Ce^{3+} as reported by Brgoch *et al.*[25] However, more than 94% of the internal QE at room temperature can be preserved for BLS:Ce^{3+} from our previous results.[28] For all solid solution samples for $Ba_9(Lu_{2-x}Y_x)Si_6O_{24}$:$Ce^{3+}$ (x = 0–2), the dependence of the normalized internal QEs on temperatures from 40 to 280°C is given in

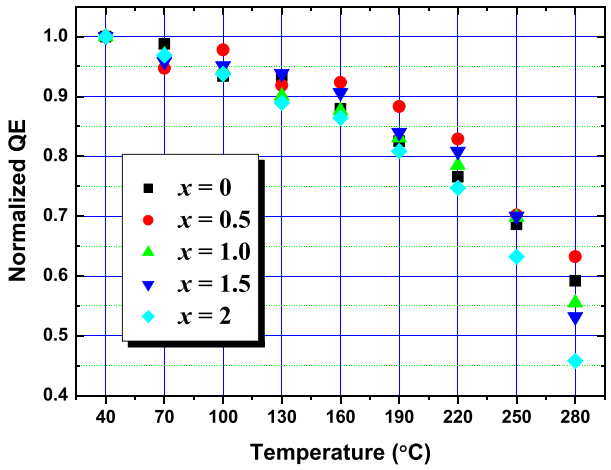

FIGURE 10 Dependence of normalized internal QEs on temperature (from 40 to 280°C) for $Ba_9(Lu_{2-x}Y_x)Si_6O_{24}:5\%Ce^{3+}$ (x = 0–2)

Figure 10. The thermal stability slightly decreased with increase in Y content, a finding that is consist with previous reports.[25,28] The higher the QE value, the better the phosphors. Therefore, the Lu series sample is more promising than the Y-series sample for application in NUV-based white LEDs.

4 | CONCLUSIONS

In summary, samples of the $Ba_9(Lu_{2-x}Y_x)Si_6O_{24}:Ce^{3+}$ (x = 0–2) blue-green phosphors were synthesized by solid-state reactions. All the samples exhibited a rhombohedral crystal structure. With increase in the Y^{3+} content, the XRD peaks shift to small angle region as Y^{3+} is larger than Lu^{3+}. Samples exhibit strong blue-green emissions around 490 nm and an intense excitation band around 400 nm that matches well with the emission light of the efficient NUV chip. With increasing Y^{3+} content, both emission and excitation give a small blue shift that resulted from weak crystal-field splitting. The luminescence intensity and QE decrease with increasing Y^{3+} concentration. The internal QE decreases from 74 to 50% and the external QE decreases from 50 to 34% as x was increased from 0 to 2. The QE and thermal stability of the Lu series sample are much higher than that of the Y-series samples. These results indicate the promising application of the Lu series samples for the NUV-based white LEDs.

ACKNOWLEDGEMENTS

This work is financially supported by the National High Technology Research and Development Program of China (863 Program) (2015AA03A101), the National Natural Science Foundation of China (U1201254, 11404351, 61306059), and the Science and Technology Planning Project of Guangdong Province (2014B010122005, 2014B010122001, 2015B010114002, 2015B010133001).

REFERENCES

[1] E. F. Schubert, J. K. Kim, *Science* **2005**, *308*, 1274.

[2] S. Pimputkar, J. S. Speck, S. P. Den Baars, S. Nakamura, *Nat. Photon.* **2009**, *34*, 180.

[3] J. Y. Tsao, M. H. Crawford, M. E. Coltrin, A. J. Fischer, D. D. Koleske, G. S. Subramania, G. T. Wang, J. J. Wierer, R. F. Karlicek, *Adv. Opt. Mater.* **2014**, *2*, 809.

[4] J. Meyer, F. Tappe, *Adv. Opt. Mater.* **2014**, *3*, 424.

[5] Y. Liu, X. Zhang, Z. Hao, W. Lu, X. Liu, X.-J. Wang, J. Zhang, *J. Phys. D: Appl. Phys.* **2011**, *44*, 075402.

[6] Y. Liu, X. Zhang, Z. Hao, Y. Luo, X.-J. Wang, J. Zhang, *J. Lumin.* **2012**, *132*, 1257.

[7] X. Zhang, Y. Liu, Z. Hao, Y. Luo, X.-J. Wang, J. Zhang, *Mater. Res. Bull.* **2012**, *47*, 1149.

[8] A. Setlur, *Electrochem. Soc. Interface.* **2009**, *18*, 32.

[9] V. Bachmann, C. Ronda, A. Meijerink, *Chem. Mater.* **2009**, *21*, 2077.

[10] P. Schlotter, R. Schmidt, J. Schneider, *Appl. Phys. A.* **1997**, *64*, 417.

[11] Z. Xia, Y. Zhang, M. S. Molokeev, V. V. Atuchin, *J. Phys. Chem. C* **2013**, *117*, 20847.

[12] Y. Jin, J. Zheng, *Mater. Lett.* **2014**, *114*, 4.

[13] W. Shen, Y. Zhu, Z. Wang, *Luminescence* **2015**, *30*, 1409.

[14] B. Yuan, Y. Song, Y. Sheng, K. Zheng, Q. Huo, X. Xu, H. Zou, *Luminescence* **2016**, *31*, 453.

[15] V. V. Rangari, V. Singh, S. J. Dhoble, *Luminescence* **2016**, *31*, 600.

[16] Y. Ma, W. Ran, W. Li, C. Ren, H. Jiang, J. Shi, *Luminescence* **2016**, *31*, 665.

[17] J. Wang, W. Zhao, *Luminescence* **2016**, doi: 10.1002/bio.3175

[18] N. Komuro, M. Mikami, Y. Shimomura, E. G. Bithell, A. K. Cheetham, *J. Mater. Chem. C* **2015**, *3*, 204.

[19] Z. Xia, Q. Liu, *Progr. Mater. Sci.* **2016**, *84*, 59.

[20] Z. Xia, G. Liu, J. Wen, Z. Mei, M. Balasubramanian, M. S. Molokeev, L. Peng, L. Gu, D. J. Miller, Q. Liu, K. R. Poeppelmeier, *J. Am. Chem. Soc.* **2016**, *138*, 1158.

[21] Y. Liu, X. Zhang, Z. Hao, X.-J. Wang, J. Zhang, *Chem. Commun.* **2011**, *47*, 10677.

[22] Y. Liu, X. Zhang, Z. Hao, Y. Luo, X.-J. Wang, J. Zhang, *J. Mater. Chem.* **2011**, *21*, 16379.

[23] Y. Liu, X. Zhang, Z. Hao, X.-J. Wang, J. Zhang, *J. Mater. Chem.* **2011**, *21*, 6354.

[24] W. Lü, N. Guo, Y. Jia, Q. Zhao, W. Lv, M. Jiao, B. Shao, H. You, *Inorg. Chem.* **2013**, *52*, 3007.

[25] J. Brgoch, C. K. H. Borg, K. A. Denault, A. Mikhailovsky, S. P. DenBaars, R. Seshadri, *Inorg. Chem.* **2013**, *52*, 8010.

[26] X. Zhang, Y. Liu, J. Lin, Z. Hao, Y. Luo, Q. Liu, J. Zhang, *J. Lumin.* **2014**, *146*, 321.

[27] S. Park, *Mater. Lett.* **2014**, *135*, 59.

[28] Y. Liu, J. Zhang, C. Zhang, J. Xu, G. Liu, J. Jiang, H. Jiang, *Adv. Opt. Mater.* **2015**, *3*, 1096.

[29] K. Song, J. Zhang, Y. Liu, C. Zhang, J. Jiang, H. Jiang, H. Qin, *J. Phys. Chem. C* **2015**, *119*, 24558.

[30] Y. Liu, J. Zhang, C. Zhang, J. Jiang, H. Jiang, *J. Phys. Chem. C* **2016**, *120*, 2362.

[31] C. Zhang, Y. Liu, J. Zhang, X. Zhang, J. Zhang, Z. Cheng, J. Jiang, H. Jiang, *Mater. Res. Bull.* **2016**, *80*, 288.

[32] Y. Liu, C. Zhang, Z. Cheng, Z. Zhou, J. Jiang, H. Jiang, *Inorg. Chem.* **2016**, *55*, 8628.

[33] P. D. Rack, P. H. Holloway, *Mater. Sci. Eng.* **1998**, *R21*, 171.

[34] J. H. Brannon, D. Magde, *J. Phys. Chem.* **1978**, *82*, 705.

[35] A. T. R. Williams, S. A. Winfield, J. N. Miller, *Analyst* **1983**, *108*, 1067.

[36] C. V. Bindhu, S. S. Harilal, G. K. Varier, R. C. Issac, V. P. N. Nampoori, C. P. G. Vallabhan, *J. Phys. D: Appl. Phys.* **1996**, *29*, 1074.

[37] J. J. Joos, J. Botterman, P. F. Smet, *J. Solid State Lighting* **2014**, *1*, 6.

[38] J. N. Demas, G. A. Crosby, *J. Phys. Chem.* **1971**, *75*, 991.

How to cite this article: Xu H, Zhou Z, Liu Y, et al. Crystal structure and luminescence properties of the blue-green-emitting $Ba_9(Lu, Y)_2Si_6O_{24}:Ce^{3+}$ phosphor. *Luminescence*. 2017;32:812–816. https://doi.org/10.1002/bio.3256